Calculation of backscatter factors for diagnostic radiology using Monte Carlo methods

1998 Phys. Med. Biol. 43 2237

(http://iopscience.iop.org/0031-9155/43/8/017)

Phys. Med. Biol. **43** (1998) 2237–2250. Printed in the UK PII: S0031-9155(98)86947-9

Calculation of backscatter factors for diagnostic radiology using Monte Carlo methods

N Petoussi-Henss, M Zankl, G Drexler, W Panzer and D Regulla

GSF-National Research Center for Environment and Health, Institute of Radiation Protection, Ingolstädter Landstrasse 1, D-85764 Neuherberg, Federal Republic of Germany

Received 18 August 1997, in final form 17 December 1997

Abstract. Backscatter factors were determined for x-ray beams relevant to diagnostic radiology using Monte Carlo methods. The phantom size considered most suitable for calibration of dosimeters is a cuboid of 30×30 cm^2 front surface and 15 cm depth. This phantom size also provides a good approximation to adult patients. Three different media were studied: water, PMMA and ICRU tissue; the source geometry was a point source with varying field size and source-to-phantom distance. The variations of the backscatter factor with phantom medium and field geometry were examined. From the obtained data, a set of backscatter factors was selected and proposed for adoption as a standard set for the calibration of dosimeters to be used to measure diagnostic reference doses.

1. Introduction

The backscatter factor is closely related to entrance surface dose. The entrance surface dose to patients in x-ray diagnosis and its measurement has been much studied in recent years, and was introduced as the dose descriptor to quantify diagnostic reference doses for radiographic examination. Diagnostic reference doses are part of the quality criteria as laid down in the *European Guidelines on Quality Criteria for Diagnostic Radiographic Images* (European Commission 1996a) and *European Guidelines on Quality Criteria for Diagnostic Radiographic Images in Paediatrics* (European Commission 1996b). They are also recommended by the International Commission on Radiological Protection (ICRP 1996) and by the IAEA (1996) as 'guidance doses'. The commitment to apply quality criteria is a consequence of the *Council Directive on Health Protection of Individuals Against the Dangers of Ionizing Radiation in Relation to Medical Exposures* (Commission of the European Communities 1997) which has to be transposed into national law by the member states of the European Community.

Diagnostic reference dose values provide quantitative guidance to help identify relatively poor or inadequate use of a technique and, consequently, the need for appropriate corrective action. They were derived for the most important examinations from the results of wide-scale field studies. In clinical practice, compliance with the reference doses should be tested by measurements on a series of representative patients. Since these measurements occur under routine examination conditions the dosimetric effort has to be kept to a minimum. In general there remain three approaches:

(i) Measurement of dose–area product (in cases where the device for this purpose is installed) and determination of entrance field size.

0031-9155/98/082237+14$19.50

(ii) Determination of entrance dose from tube output measurements (in cases of manual setting of exposure time and tube current or when the tube current × exposure time (mA s) value governed by the automatic exposure control unit is displayed).

(iii) Direct measurement of entrance surface dose by means of solid state detectors (thermoluminescence dosimeters, diodes etc).

In all the above situations knowledge of backscatter factors (BSF) is indispensable: in the first two cases to calculate entrance surface dose from the scatter-free entrance dose and in the third case to calibrate the solid state dosimeters. Due to constraints imposed by their construction, these dosimeters are energy and direction dependent and have therefore to be calibrated on phantoms under typical exposure conditions. To this end, however, there exist scarcely any suitable reference dosimeters. Ionization dosimeters for x-ray diagnosis which might act as reference instruments are generally designed and calibrated for free-in-air measurements.

Backscatter factors reported in the literature mostly stem from measurements (*British Journal of Radiology* 1953, 1961, 1972, 1983, Harrison 1982, IAEA 1987, Klevenhagen 1982, 1989) but also from theoretical calculations (Chan and Doi 1983, Grosswendt 1984, 1990, 1993, Bartlett *et al* 1990).

It is known that the backscatter factor depends on the x-ray spectrum, the field geometry, the dimension of the phantom and its material (e.g. Harrison 1982, Grosswendt 1990, 1993, Carlsson 1993).

The aim of the present work is to complement the already existing knowledge on BSF in diagnostic radiology and to provide a basic data set for the determination of BSF for spectral distributions which occur in radiographic examinations to be used for: (i) the calibration of solid state dosimeters as already mentioned, (ii) for the assessment of organ doses in x-ray diagnosis from measured surface doses by applying conversion coefficients which are normalized to air kerma free-in-air.

For the purposes of this work, the calculation of the BSF was carried out using Monte Carlo methods and mathematical phantoms of a rectangular shape with a homogeneous material composition of water, ICRU tissue or PMMA. The usual diagnostic irradiation conditions were considered, regarding beam qualities and geometries. The calculated BSF would vary accordingly and it is necessary to know the amount of variation that occurs for the several materials and irradiation geometries, as well as for the photon energy range.

The Monte Carlo method for the determination of BSF was chosen because measurements at diagnostic x-ray units demand high experimental effort, cannot cover the occurring variety of radiation qualities and are hampered by a lack of suitable reference dosimeters and traceable calibration factors.

2. Definition

The BSF has been derived differently for different purposes and by various workers.

Backscatter factor is generally considered the ratio between a dose quantity measured at a phantom or material surface which is facing the source of radiation and the same dose quantity at the same position free in air. Consequently, the BSF could be defined as follows:

(i) The BSF is defined as the ratio of the air kerma on the surface of a phantom (consisting, for example, of water, ICRU tissue or PMMA), to the air kerma free-in-air, i.e. the kerma to air in the same point in space in the absence of the phantom. This definition in the case of a water phantom was adopted, for example by the IAEA code of practice (IAEA 1987).

An alternative definition is as follows:

(ii) The BSF is alternatively defined as the ratio of the kerma to tissue (i.e. water, ICRU tissue or PMMA) on the surface of the phantom consisting of the same material, to the kerma to tissue at the same point in space in the absence of the phantom. This definition with water as the phantom and reference material was adopted by IPSM (1991) and IPEMB (1996). It was extended to other materials by Grosswendt (1984, 1990, 1993) for his Monte Carlo calculations.

The numerical values of BSF vary depending on both the definition used and the reference and phantom material chosen.

Dosimetry in x-ray diagnosis is an air kerma domain. Typically all in-beam dose measurements (dose–area product, output, entrance dose, dose at the imaging system) are performed with dosimeters specially designed for their respective purpose and calibrated in terms of air kerma. Reference doses as existing up to now are also given in air kerma (European Commission 1996a, b). Finally, the determination of organ doses or effective dose is based on entrance dose or dose–area product. Consequently, the first definition is the one with the most direct connection to dosimetry in x-ray diagnosis and was, therefore, adopted for this work.

3. Method

For the simulation of the transport of the photons in phantoms a Monte Carlo code called KASTENSPEC (Petoussi *et al* 1990), developed at the GSF, was used. The photon interactions considered were photoelectric absorption, Compton scattering and pair production. Rayleigh scattering was not considered, but this effect is of no importance for the purpose of this study. The appropriate cross-sectional data for the media considered were combined from those for single elements (Roussin *et al* 1983) according to the composition of the media. The kerma approximation was assumed, i.e. the energy transferred at a point of inelastic photon interaction was deposited at that point and secondary electrons were not pursued further. This assumption is valid as long as there is approximate electron equilibrium which can be assumed, for the tissues involved, for all photon energies considered in this study.

A cuboid phantom of front surface 30×30 cm^2 and depth 15 cm was simulated and calculations were performed for three different phantom media: water, polymethylmethacrylate (PMMA; elemental composition by mass 8% H, 60% C and 32% O; density 1.19 g cm^{-3}) and ICRU tissue (elemental composition by mass 10.1% H, 11.1% C, 2.6% N and 76.2% O; density 1.0 g cm^{-3}). The phantoms were suspended in a vacuum. For the purpose of this work, this phantom thickness approximates adult patients in x-ray diagnosis. Furthermore, it provides full backscatter (Klevenhagen 1982).

ICRU Report 47 (ICRU 1992) suggested a PMMA slab phantom of the above size as a suitable calibration phantom for personal dosimeters in order to achieve uniformity in calibration procedures. However, PMMA is not strictly tissue equivalent and hence the water-filled thin-walled PMMA phantom recommended by the International Standardization Organization (1995) is a practical and cheap alternative.

The irradiation geometries simulated were point source geometries with focus-to-skin distances (FSD) of 50, 100 and 150 cm and field sizes of 10×10 cm^2, 20×20 cm^2 and 25×25 cm^2.

The choice of phantom materials and size is meant to meet the calibration needs. Considering the irradiation geometries, the focus-to-skin distances selected for simulation

range from a short one to a more remote one in order to study the variations FSD may induce on the BSF. The FSD of 100 cm represents a typical value in diagnostic radiology. Similarly the field sizes cover the range of fields in practice.

The backscatter factor was evaluated by the ratio of air kerma on the surface of the phantom to the air kerma free-in-air (see definition (i)). The kerma was evaluated by converting the photon fluence at the centre of the phantom's entrance surface to kerma at this plane. For the evaluation of photon fluence, a planar scoring square with 1 cm^2 dimension was defined, centred on the front surface, and the angle of intersection of a photon with this planar area was appropriately taken into consideration. The air kerma was then deduced from the photon fluence by multiplying with the photon energy and the appropriate mass energy absorption coefficient of air. The latter absorption coefficients were evaluated from those given for single elements (Hubbell 1982) according to the elemental composition. More details can be found in Till *et al* (1995).

By performing the calculation using the photon fluence in a scoring area instead of the deposited energy in collective volumes, a higher statistical accuracy can be achieved. Fifty million histories were run for each phantom, for a given geometry and incident energy. The random uncertainty resulting from Monte Carlo statistics (i.e. coefficient of variance) was generally less than 1%.

The Monte Carlo calculations were performed for 14 monoenergetic beams between 0.01 and 1 MeV. Higher energies than those relevant in diagnostic radiology were considered for the sake of completeness. The BSF for intermediate energies were evaluated by fitting a cubic spline curve through the calculated data; those for spectral beams were then estimated by folding the spectral energy distribution with the monochromatic BSF values according to the formula

$$\overline{\mathrm{BSF}} = \frac{\int_E \varphi(E) E (\mu_{\mathrm{en}}(E)/\rho) \mathrm{BSF}(E)\, \mathrm{d}E}{\int_E \varphi(E) E (\mu_{\mathrm{en}}(E)/\rho)\, \mathrm{d}E} \tag{1}$$

where $\varphi(E)$ is the number of photons with energy E, $\mu_{\mathrm{en}}(E)$ is the mass energy absorption coefficient of air for energy E, ρ is the mass density of air and BSF(E) is the monoenergetic backscatter factor.

The spectral distribution of particle number and fluence of the backscattered photons was calculated for energy increments of generally 1 keV.

4. Results and discussion

Tables 1–3 show the monoenergetic data of backscatter factors for the point source geometries considered and for water, ICRU tissue and PMMA respectively. They form the basic data set from which the BSF for any spectral beam in the energy range considered can be folded using formula (1).

Figures 1–3 show graphically a selection of these data: figure 1 presents the backscatter factors for water, ICRU tissue and PMMA tissue for the monoenergetic beams, as a function of incident photon energy. The FSD is 100 cm and the field size 20 × 20 cm^2. It can be seen that the BSF for water is lower than for ICRU tissue and always lower than the BSF for PMMA: the highest deviation is observed at 20–30 keV where the difference in BSF is about 1% between the water and the ICRU tissue values and 8% between the water and PMMA values; in the maximum backscatter energy region, around 60 keV, the differences in BSF are about 1% and up to 7% respectively, whereas above 150 keV, deviations up to 0.5% and 3% are observed. Generally, it can be seen that the PMMA phantom introduces

Table 1. Backscatter factors for water for three field sizes and three FSDs.

Photon energy (keV)	FSD 50 cm			FSD 100 cm			FSD 150 cm		
	10 × 10 (cm^2)	20 × 20 (cm^2)	25 × 25 (cm^2)	10 × 10 (cm^2)	20 × 20 (cm^2)	25 × 25 (cm^2)	10 × 10 (cm^2)	20 × 20 (cm^2)	25 × 25 (cm^2)
0.010	1.01	1.01	1.02	1.01	1.01	1.02	1.01	1.01	1.01
0.020	1.11	1.11	1.11	1.11	1.11	1.11	1.11	1.11	1.11
0.030	1.26	1.27	1.28	1.27	1.28	1.28	1.27	1.28	1.28
0.040	1.41	1.47	1.47	1.41	1.48	1.48	1.42	1.48	1.48
0.050	1.47	1.58	1.61	1.48	1.61	1.62	1.49	1.61	1.65
0.060	1.47	1.62	1.64	1.48	1.64	1.68	1.49	1.64	1.70
0.070	1.45	1.60	1.64	1.47	1.63	1.66	1.46	1.63	1.70
0.080	1.40	1.55	1.58	1.41	1.58	1.61	1.41	1.58	1.64
0.100	1.33	1.46	1.49	1.34	1.49	1.52	1.34	1.49	1.53
0.150	1.22	1.32	1.34	1.23	1.34	1.36	1.23	1.34	1.37
0.200	1.17	1.24	1.26	1.17	1.26	1.28	1.17	1.27	1.29
0.300	1.11	1.16	1.18	1.12	1.17	1.19	1.12	1.18	1.19
0.500	1.07	1.10	1.11	1.07	1.11	1.12	1.07	1.11	1.12
1.000	1.03	1.05	1.05	1.03	1.05	1.05	1.03	1.05	1.05

Table 2. Backscatter factors for ICRU tissue for three field sizes and three FSDs.

Photon energy (keV)	FSD 50 cm			FSD 100 cm			FSD 150 cm		
	10 × 10 (cm^2)	20 × 20 (cm^2)	25 × 25 (cm^2)	10 × 10 (cm^2)	20 × 20 (cm^2)	25 × 25 (cm^2)	10 × 10 (cm^2)	20 × 20 (cm^2)	25 × 25 (cm^2)
0.010	1.02	1.02	1.02	1.02	1.02	1.02	1.02	1.02	1.02
0.020	1.12	1.11	1.11	1.11	1.12	1.11	1.12	1.12	1.12
0.030	1.28	1.29	1.29	1.28	1.29	1.30	1.28	1.30	1.30
0.040	1.42	1.48	1.49	1.42	1.50	1.51	1.42	1.50	1.50
0.050	1.48	1.60	1.62	1.49	1.63	1.64	1.49	1.64	1.67
0.060	1.48	1.63	1.66	1.49	1.66	1.69	1.49	1.66	1.72
0.070	1.46	1.61	1.65	1.47	1.63	1.68	1.47	1.63	1.70
0.080	1.40	1.55	1.59	1.41	1.58	1.63	1.41	1.58	1.64
0.100	1.33	1.46	1.49	1.34	1.49	1.53	1.34	1.50	1.54
0.150	1.22	1.32	1.34	1.23	1.34	1.36	1.23	1.34	1.37
0.200	1.17	1.24	1.27	1.17	1.25	1.28	1.18	1.27	1.29
0.300	1.11	1.16	1.18	1.12	1.17	1.19	1.12	1.18	1.19
0.500	1.07	1.10	1.11	1.07	1.10	1.12	1.07	1.10	1.12
1.000	1.03	1.05	1.05	1.03	1.05	1.05	1.03	1.05	1.05

high backscatter factors at energies below 150 keV which could deviate from those of water up to 8%, depending on the quality of the beam (see also tables 1–3).

In figure 2 the effect of focus-to-skin distance (FSD) is demonstrated: BSF for the water (figure 2(a)) and the PMMA (figure 2(b)) slab phantoms for point sources with FSD 150, 100 and 50 cm respectively and the same field area are shown. It can be seen that, for the water phantom, the fluctuation of FSD in the above range does not influence the BSF significantly: although the higher the FSD, the higher the BSF, the variations are small, in the range of 2%. This is also in agreement with the findings of Grosswendt (1990). The situation with the PMMA phantom (figure 2(b)) is very similar but the differences are (a couple of per cent) more pronounced.

Table 3. Backscatter factors for PMMA for three field sizes and three FSDs.

Photon energy (keV)	FSD 50 cm			FSD 100 cm			FSD 150 cm		
	10×10 (cm^2)	20×20 (cm^2)	25×25 (cm^2)	10×10 (cm^2)	20×20 (cm^2)	25×25 (cm^2)	10×10 (cm^2)	20×20 (cm^2)	25×25 (cm^2)
0.010	1.02	1.02	1.02	1.02	1.02	1.02	1.02	1.02	1.02
0.020	1.17	1.16	1.16	1.16	1.16	1.16	1.16	1.17	1.16
0.030	1.36	1.38	1.38	1.36	1.39	1.40	1.36	1.40	1.40
0.040	1.51	1.60	1.59	1.52	1.62	1.64	1.52	1.63	1.64
0.050	1.57	1.72	1.76	1.59	1.75	1.77	1.59	1.76	1.80
0.060	1.56	1.74	1.78	1.57	1.77	1.81	1.58	1.77	1.83
0.070	1.53	1.72	1.74	1.54	1.74	1.78	1.54	1.74	1.81
0.080	1.46	1.64	1.69	1.48	1.68	1.72	1.47	1.71	1.74
0.100	1.38	1.53	1.56	1.38	1.55	1.59	1.39	1.56	1.60
0.150	1.25	1.36	1.38	1.26	1.37	1.40	1.26	1.37	1.41
0.200	1.19	1.27	1.29	1.20	1.29	1.31	1.20	1.29	1.31
0.300	1.12	1.18	1.20	1.13	1.19	1.21	1.13	1.20	1.21
0.500	1.07	1.11	1.11	1.08	1.11	1.13	1.08	1.13	1.13
1.000	1.03	1.05	1.05	1.04	1.06	1.06	1.04	1.06	1.06

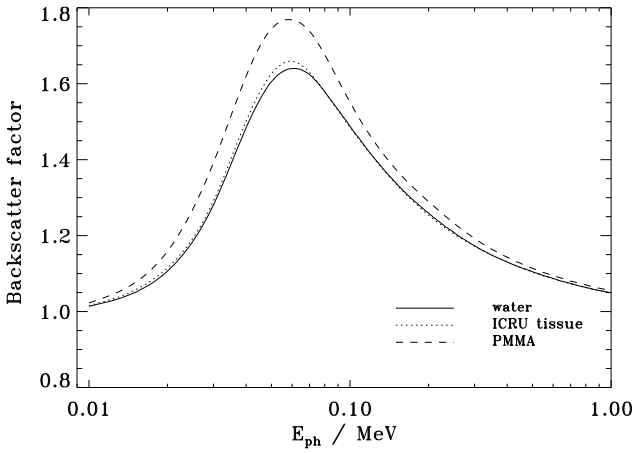

Figure 1. Backscatter factors as a function of primary monoenergetic photons, on the surface of a water, ICRU tissue and PMMA slab phantom with size $30 \times 30 \times 15$ cm^3, irradiated with point beams: field size 20×20 cm^2; FSD 100 cm.

Similarly, figures 3(a) and 3(b) show the BSF for the water and PMMA phantom respectively, for three different field sizes, 25×25 cm^2, 20×20 cm^2 and 10×10 cm^2, all for FSD 100 cm. As expected, the BSF for the bigger field are higher than for the smaller one, reflecting the increasing number of photons scattered back from the phantom; for water, the differences between the BSFs for the 10×10 cm^2 area and the 25×25 cm^2 area are up to 12%. The situation is similar for the PMMA phantom (figure 3(b)) but the deviations are slightly higher, up to 14%.

Table 4 shows the backscatter factors for water, ICRU and PMMA tissue for the most common spectral beams used in diagnostic radiology and for an FSD of 100 cm, which is a standard calibration distance, and three field sizes, covering small to bigger irradiation areas.

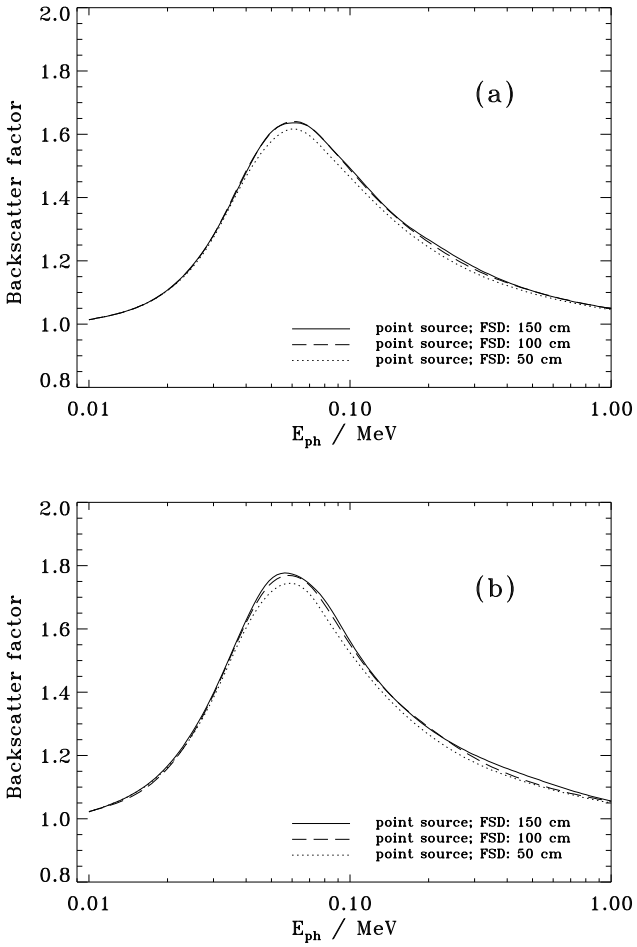

Figure 2. Backscatter factors as a function of primary monoenergetic photons, on the surface of a water (a) and PMMA (b) slab phantom with size $30 \times 30 \times 15$ cm^3 irradiated from various FSD. The field size is 20×20 cm^2.

The spectra as they emerge from the x-ray tube were simulated using the well established semiempirical method of Birch and Marshall (1979).

Figure 4 demonstrates graphically the influence of the radiation quality on the backscatter factor, by showing the BSF as a function of the half-value layer (HVL) aluminium for the water slab phantom, FSD 100 cm and field size 20×20 cm^2. It can be seen that in the energy range considered, and for a given filtration, the backscatter factor increases with increasing HVL due to the increasing proportion of photons in the energy range 50–70 keV, where the monoenergetic BSF is highest. Figure 4 also shows that the HVL in this energy range can be considered as a suitable descriptor of radiation quality with respect to the backscatter factor.

Figure 5 shows the spectrum of backscattered photons (called 'backscattered spectrum' in the following) on the surface of the water cuboid phantom for a beam generated by 80 kV tube voltage and filtered with 2.5 mm Al; figure 6 shows the backscattered spectrum for 150 kV tube voltage and 3 mm Al + 0.1 mm Cu filtration for PMMA as phantom material.

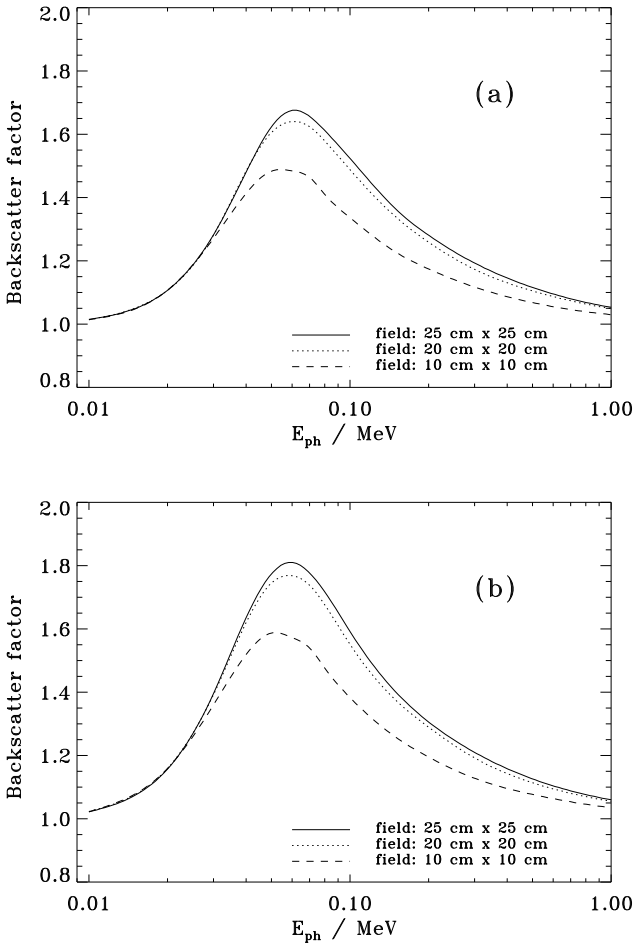

Figure 3. Backscatter factors as a function of primary monoenergetic photons, on the surface of a water (a) and PMMA (b) slab phantom with size $30 \times 30 \times 15$ cm^3 irradiated with three different field areas; FSD 100 cm.

The FSD and field size were 100 cm and 20×20 cm^2 respectively. In the same figures, the incident and surface spectra (i.e. incident plus backscattered) are also shown. It can be seen that the backscattered spectrum does not include photons softer than the incident. More x-ray spectra at the surface and at various depths in water and lung phantoms were given in an earlier work (Petoussi *et al* 1990).

Table 5 shows the dependence of mean energy of the backscattered spectra on the beam quality and phantom material. It reveals that the mean energy decreases by 8–25% in the energy range considered, the more pronounced decrease being observed for PMMA and the higher incident mean energy. This has the consequence that the demands on energy dependence of reference dosimeters as well as detectors to be calibrated do not differ for backscattered and incident spectra.

It is difficult to make a direct comparison of the present data with other published data since almost every author has considered other phantom or irradiation conditions. Table 6 shows a comparison with the data of Bartlett *et al* (1990), stemming from Monte Carlo

Table 4. Backscatter factors for water, ICRU tissue and PMMA for some spectral beams typical in diagnostic radiology and for three field sizes and FSD of 100 cm.

				Field: 10 × 10 cm^2			Field: 20 × 20 cm^2			Field: 25 × 25 cm^2		
Tube voltage (kV)	Filter	HVL (mm Al)	Mean energy (keV)	BSF water	BSF ICRU tissue	BSF PMMA	BSF water	BSF ICRU tissue	BSF PMMA	BSF water	BSF ICRU tissue	BSF PMMA
50	2.5 mm Al	1.74	32.0	1.24	1.25	1.33	1.26	1.27	1.36	1.26	1.28	1.36
60	2.5 mm Al	2.08	35.8	1.28	1.28	1.36	1.31	1.32	1.41	1.31	1.32	1.42
70	2.5 mm Al	2.41	39.3	1.30	1.31	1.39	1.34	1.36	1.45	1.35	1.36	1.46
70	3.0 mm Al	2.64	40.0	1.32	1.32	1.40	1.36	1.37	1.47	1.36	1.38	1.48
70	3.0 mm Al + 0.1 mm Cu	3.96	44.0	1.38	1.39	1.48	1.45	1.47	1.58	1.46	1.47	1.59
80	2.5 mm Al	2.78	42.9	1.32	1.33	1.41	1.37	1.39	1.48	1.38	1.39	1.50
80	3.0 mm Al	3.04	43.7	1.34	1.34	1.42	1.39	1.40	1.51	1.40	1.41	1.52
80	3.0 mm Al + 0.1 mm Cu	4.55	48.2	1.40	1.40	1.49	1.48	1.50	1.61	1.49	1.51	1.63
90	2.5 mm Al	3.17	46.3	1.34	1.34	1.43	1.40	1.41	1.51	1.41	1.42	1.53
90	3.0 mm Al	3.45	47.0	1.35	1.36	1.44	1.42	1.43	1.53	1.42	1.44	1.55
90	3.0 mm Al + 0.1 mm Cu	5.12	51.7	1.41	1.41	1.50	1.50	1.51	1.62	1.51	1.53	1.65
100	2.5 mm Al	3.24	48.1	1.34	1.34	1.42	1.40	1.41	1.51	1.41	1.42	1.53
100	3.0 mm Al	3.88	50.0	1.36	1.37	1.45	1.44	1.45	1.55	1.45	1.46	1.57
100	3.0 mm Al + 0.1 mm Cu	5.65	54.8	1.41	1.42	1.50	1.51	1.53	1.64	1.53	1.55	1.66
110	2.5 mm Al	3.59	50.8	1.35	1.35	1.43	1.42	1.43	1.53	1.43	1.44	1.55
120	3.0 mm Al	4.73	55.4	1.37	1.38	1.46	1.46	1.48	1.58	1.48	1.49	1.60
120	3.0 mm Al + 0.1 mm Cu	6.62	60.1	1.41	1.42	1.50	1.53	1.54	1.64	1.54	1.56	1.67
130	2.5 mm Al	4.32	55.6	1.36	1.36	1.44	1.44	1.45	1.55	1.45	1.47	1.57
150	2.5 mm Al	4.79	59.1	1.36	1.36	1.44	1.45	1.46	1.55	1.46	1.48	1.58
150	3.0 mm Al	6.80	64.9	1.39	1.39	1.47	1.50	1.51	1.61	1.52	1.53	1.63
150	3.0 mm Al + 0.1 mm Cu	8.50	69.2	1.40	1.41	1.48	1.53	1.54	1.64	1.55	1.57	1.67

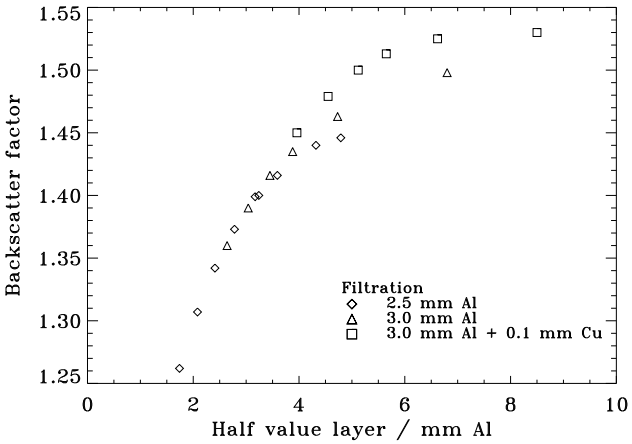

Figure 4. Backscatter factor as a function of half-value layer in mm Al, for a water slab phantom with size $30 \times 30 \times 15$ cm^3; FSD 100 cm; field size 20×20 cm^2.

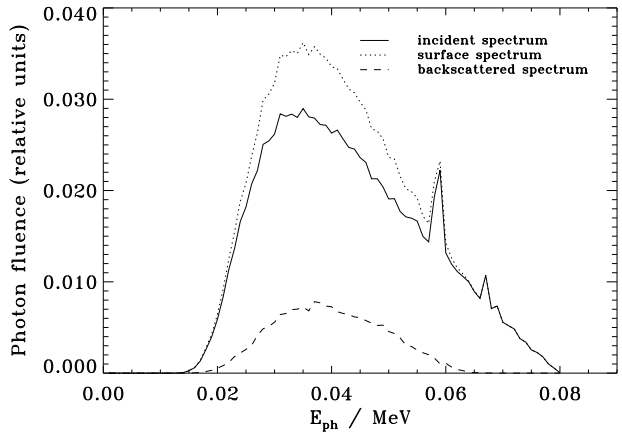

Figure 5. Spectra on the surface of a $30 \times 30 \times 15$ cm^3 water phantom for 80 kV tube voltage and 2.5 mm Al filtration. FSD 100 cm; field size 20×20 cm^2.

calculations for the ICRU tissue and PMMA slab phantom of size $30 \times 30 \times 15$ cm^3. For this comparison, the beam geometry used by Bartlett *et al* (1990), i.e. full irradiation of the phantom by a broad parallel beam, was replicated. It can be seen that the agreement of both data sets is excellent.

All the BSF shown in tables 1–6 and figures 1–6 are derived by considering definition (i) i.e. air is the reference material.

Table 7 presents a comparison with results from Harrison (1982) who measured BSF on the surface of a water tank for an FSD of 60 cm, different field sizes and a variety of x-ray spectra using an ionization chamber. These spectra, characterized by tube voltage, added filtration and HVL, were simulated by the method of Birch and Marshall (1979) and combined with the monochromatic BSF values of this work using formula (1). The data from this work were selected to fit the situation of Harrison (1982) most closely, i.e. an FSD of 50 cm, 10×10 cm^2 field size and water as phantom material. The agreement shown

Table 5. Mean energies of incident spectra and of the resulting backscattered spectra, at the surface of the water, ICRU tissue and PMMA phantoms, for some x-ray spectra beams and point source geometry: FSD 100 cm; field size 20 × 20 cm^2.

			Mean energy (keV)			
				Backscattered spectra on		
Tube voltage (kV)	Filter	HVL (mm Al)	Incident spectrum	Water	ICRU tissue	PMMA
80	2.5 mm Al	2.78	42.9	39.7	39.5	38.7
100	3.0 mm Al + 0.1 mm Cu	5.65	54.8	46.3	46.0	45.0
150	3.0 mm Al + 0.1 mm Cu	8.50	69.2	54.0	53.7	52.5

Table 6. Comparison of backscatter factors calculated for this work with those from Bartlett *et al* (1990), for a cuboid ICRU tissue and PMMA slab phantom and monoenergetic broad unidirectional parallel beams incident normally.

	Backscatter factor			
Energy (MeV)	ICRU slab (present work)	ICRU slab (Bartlett *et al* 1990)	PMMA slab (present work)	PMMA slab (Bartlett *et al* 1990)
0.015	1.04	1.04	1.08	1.06
0.025	1.20	1.20	1.28	1.29
0.050	1.67	1.67	1.81	1.81
0.075	1.69	1.68	1.79	1.80
0.100	1.58	1.55	1.65	1.63
0.150	1.40	1.38	1.45	1.43

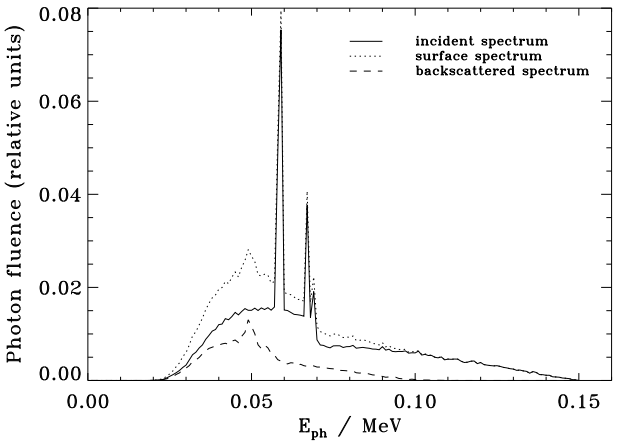

Figure 6. Spectra on the surface of a 30 × 30 × 15 cm^3 PMMA phantom for 150 kV tube voltage and 3 mm Al + 0.1 mm Cu filtration. FSD 100 cm; field size 20 × 20 cm^2.

in table 7 is excellent, i.e. generally within 0.8% with a maximum deviation of 2.5% for 60 kV and added filtration of 0.55 mm Al.

Table 7. Comparison of backscatter factors calculated for this work (FSD 50 cm) with those measured by Harrison (1982) (FSD 60 cm) for a water phantom and a field size of 10×10 cm^2.

Spectrum		Backscatter factor	
Tube voltage (kV)	Added filtration (mm Al)	Harrison (1982)	This work
60	0.00	1.18	1.19
60	0.55	1.20	1.23
60	1.00	1.25	1.25
60	2.00	1.27	1.28
75	0.00	1.22	1.23
75	0.55	1.26	1.26
75	1.00	1.29	1.28
75	2.00	1.32	1.32
90	0.00	1.25	1.26
90	0.55	1.28	1.29
90	1.00	1.31	1.31
90	2.00	1.34	1.34
100	0.00	1.27	1.27
100	0.55	1.30	1.31
100	1.00	1.34	1.32
100	2.00	1.36	1.35

Table 8. Comparison of backscatter factors calculated for this work with those from Grosswendt (1993), for a water phantom and monoenergetic point sources.

	FSD 100 cm			
Energy (MeV)	GSF values (Field: quadratic 313 cm^2)	Grosswendt (Field: circular 314 cm^2)	GSF values (Field: quadratic 79 cm^2)	Grosswendt (Field: circular 79 cm^2)
0.200	1.247	1.240	1.159	1.157
0.400	1.127	1.123	1.080	1.078
0.661	1.074	1.070	1.048	1.045
	FSD 50 cm			
Energy (MeV)	GSF values (Field: quadratic 313 cm^2)	Grosswendt (Field: circular 314 cm^2)	GSF values (Field: quadratic 79 cm^2)	Grosswendt (Field: circular 79 cm^2)
0.200	1.244	1.228	1.157	1.154
0.400	1.118	1.117	1.078	1.078
0.661	1.070	1.068	1.045	1.044

In order to make a further validation of the present calculational procedure and results, calculations were made to simulate some irradiation conditions for which Grosswendt (1993) gave values of BSF, applying Monte Carlo methods. Grosswendt calculated backscatter factors for a cylindrical water phantom, 33 cm in diameter and thickness along the central beam direction of 20 cm, point sources and circular irradiation fields. Table 8 summarizes the comparison. It can be seen that the agreement is very good: the highest discrepancy is 1.9% at 200 keV and an FSD of 50 cm. In all other cases, the differences are less than 0.6%.

The above BSF (Harrison 1982, Grosswendt 1993) were defined according to definition (ii), i.e. they are kerma-based backscatter factors for the water phantom with water as the reference material. It should be noted that the different definition of BSF when the phantom material is water does not introduce discrepancies in the numerical values of BSF. This holds also for the difference in phantom geometry encountered between the situation simulated by Grosswendt (1993) and that simulated in this work.

5. Conclusions

This work provides a set of air kerma-based backscatter factors to be used in diagnostic radiology. These values were derived for situations common in diagnostic x-ray practice concerning beam quality and exposure geometry. They are aimed to complement the data already existing from various authors with respect to field size, focus-to-surface distance, phantom dimension and material as well as radiation quality. Furthermore, BSFs for monoenergetic photons are given which allow a BSF for any spectral beam in the investigated energy range to be folded using appropriate interpolation for intermediate energies.

The results show that the focus-to-surface distance does not have a great influence on the BSF in the range considered for this work, whereas the field size has: the larger the field area, the higher the BSF. Furthermore, the values presented show once more that PMMA is not strictly tissue equivalent: while ICRU tissue results in backscatter factors almost identical to those of water, PMMA introduces higher BSFs. Thus, the use of dosimeters calibrated on a PMMA phantom for the measurement of entrance surface doses on real patients may lead to deviations of the measured doses from the true values up to approximately 8%.

The energy distribution of the backscattered photons has also been investigated. It shows that, with respect to energy dependence, no stricter demands are imposed on the detectors used than those due to the incident radiation.

Finally, it can be concluded that application of the backscatter factors of this work in practice will aid the calibration of solid state dosimeters used to measure the diagnostic reference doses as recommended recently by various international bodies.

References

Bartlett D T, Dimbylow P J and Francis T M 1990 Calculated backscatter from phantoms for photon dosemeter calibration *Radiat. Protect. Dosim.* **32** 123–5

Birch R and Marshall M 1979 Computation of bremsstrahlung X-ray spectra and comparison with spectra measured with a Ge(Li) detector *Phys. Med. Biol.* **24** 505–17

British Journal of Radiology 1953 Central axis depth dose data *Br. J. Radiol.* (suppl 5)

——1961 Depth dose tables for use in radiotherapy *Br. J. Radiol.* (suppl 10)

——1972 Central axis depth dose data for use in radiotherapy *Br. J. Radiol.* ed M Cohen, D E A Jones and D Greene (suppl 11)

——1983 Central axis depth dose data for use in radiotherapy *Br. J. Radiol.* (suppl 17)

Carlsson C A 1993 Differences in reported backscatter factors for low-energy x-rays: a literature study *Phys. Med. Biol.* **38** 521–31

Chan H-P and Doi K 1983 The validity of Monte Carlo simulation in studies of scattered radiation in diagnostic radiology *Phys. Med. Biol.* **28** 109–29

Commission of the European Communities 1997 Council Directive 97/43/Euratom on health protection of individuals against the dangers of ionizing radiation in relation to medical exposures *Official Journal of the European Communities* **L 180** 22–7

European Commission 1996a *European Guidelines on Quality Criteria for Diagnostic Radiographic Images* EUR 16260 (Luxembourg: European Commission)

European Commission 1996b *European Guidelines on Quality Criteria for Diagnostic Radiographic Images in Paediatrics* EUR 16261 (Luxembourg: European Commission)

Grosswendt B 1984 Backscatter factors for x-rays generated at voltages between 10 and 100 kV *Phys. Med. Biol.* **29** 579–91

——1990 Dependence of the photon backscatter factor for water on source-to-phantom distance and irradiation field size *Phys. Med. Biol.* **35** 1233–45

——1993 Dependence of the photon backscatter factor for water on irradiation field size and source-to-phantom distances between 1.5 and 10 cm *Phys. Med. Biol.* **38** 305–10

Harrison R M 1982 Backscatter factors for diagnostic radiology (1–4 mm Al HVL) *Phys. Med. Biol.* **27** 1465–74

Hubbell J H 1982 Photon mass attenuation and energy absorption coefficients from 1 keV to 20 MeV *Int. J. Appl. Radiat. Isot.* **33** 1269–90

IAEA 1987 Absorbed dose determination in photon and electron beams *International Atomic Energy Agency Technical Report* 277 (Vienna: IAEA)

——1996 International basic safety standards for protection against ionizing radiation and for the safety of radiation sources *International Atomic Energy Agency Safety Series* no 115 (Vienna: IAEA)

ICRP 1996 Radiological protection and safety in medicine *ICRP Publication* 73 (*Ann. ICRP* **26** (2)) (Oxford: Pergamon)

ICRU 1992 Measurements of dose equivalents from external photon and electron radiation *ICRU Report* 47 (Bethesda, MD: ICRU)

International Standardization Organization 1995 Reference photon radiations. Calibration of area and personal dosimeters for the determination of their response as a function of photon energy and angle of incidence *ISO Report* CDV 4037-3

IPEMB 1996 The IPEMB code of practice for the determination of absorbed dose for x-rays below 300 kV generating potential (0.035 mm Al–4 mm Cu HVL; 10–300 kV generating potential) *Phys. Med. Biol.* **41** 2605–25

IPSM 1991 Report of the IPSM working party on low- and medium-energy x-ray dosimetry *Phys. Med. Biol.* **36** 1027–38

Klevenhagen S C 1982 The build-up of backscatter in the energy range 1 mm Al to 8 mm Al HVL *Phys. Med. Biol.* **27** 1035–43

——1989 Experimentally determined backscatter factors for x-rays generated at voltages between 16 and 140 kV *Phys. Med. Biol.* **34** 1871–82

Petoussi N, Zankl M, Panzer W and Drexler G 1990 A catalogue of photon spectra inside water or lung phantoms *GSF Report* 40/90 (Neuherberg, Germany: GSF-National Research Center for Environment and Health, Institute of Radiation Protection)

Roussin R W, Knight J R, Hubbell J H and Howerton R J 1983 Description of the DLC-99/HUGO package of photon interaction data in ENDF/B-V format *Report no* ORNL-RSIC-46 (ENDF-335) (Oak Ridge, TN: Oak Ridge National Laboratory, Radiation Shielding Information Center)

Till E, Zankl M and Drexler G 1995 Angular dependence of depth doses in a tissue slab irradiated with monoenergetic photons *GSF Report* 27/95 (Neuherberg, Germany: GSF-National Research Center for Environment and Health, Institute of Radiation Protection)